Appendix A

ICM6 variance preserving spectra

The variance preserving spectra for kinetic energy (left panels) and temperature (right panels) for the ICM6 current meter observations are presented herein. The observations were detrended by the mean before the spectra calculation. The length of the shortest record was 363 days while the longest one was 641 days. Number of observations (n) are indicated on the top left corner of each plot. Sampling interval is 6 h. Block averaging and overlap was used to improve the statistical reliability of the spectral estimates, as indicated below:

Bold line (black)

Number of pieces: 6
Points/piece: 720 (120 days)
Overlap: 360 (60 days)

Thin line (gray)

Number of pieces: 6
Points/piece: n (time series length)
Overlap: n/2 (half of the time series length)

Corrigendum: Temperature spectra units (right) are $°C^2$ (instead of $cm^2\ s^{-2}$)

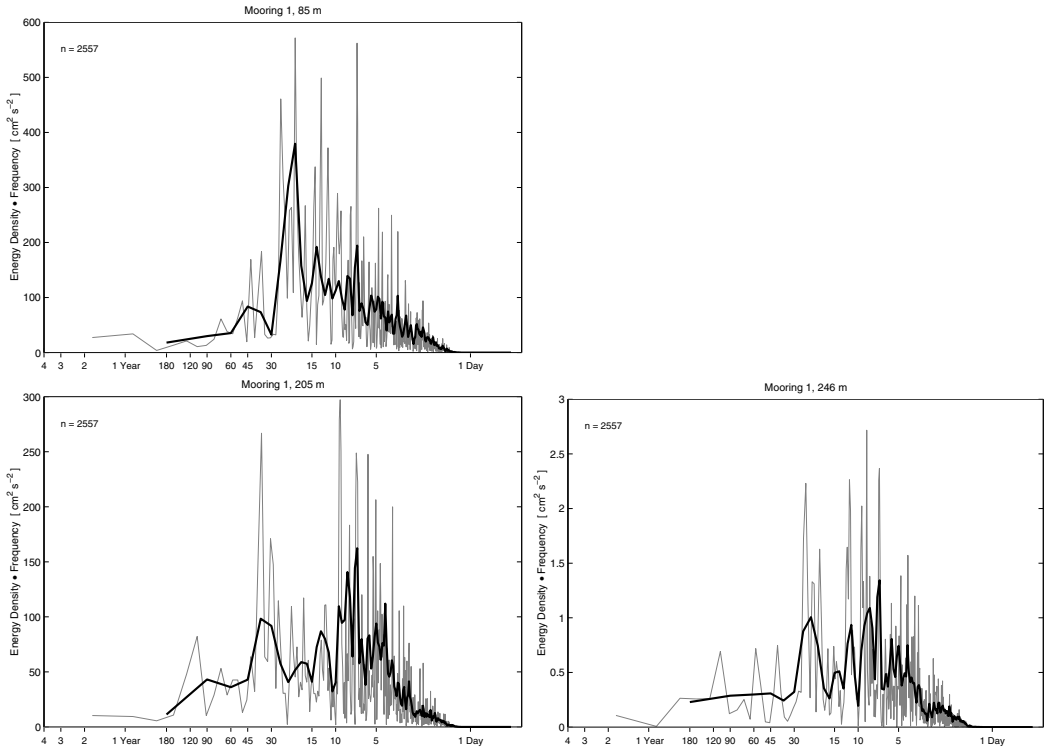

Figure A.1. Kinetic energy (left) and temperature (right) variance preserving spectra from ICM6 mooring 1.

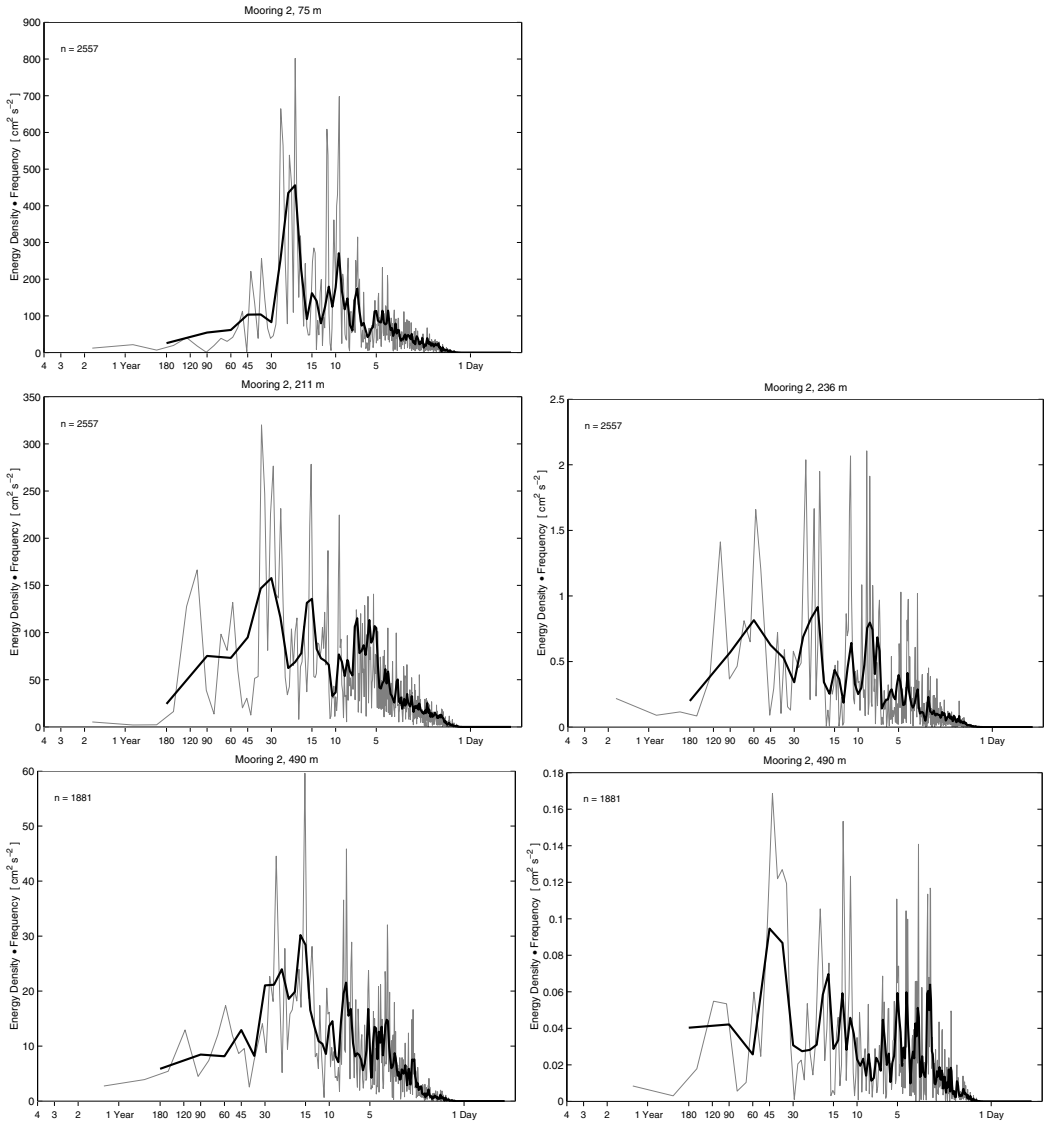

Figure A.2. Kinetic energy (left) and temperature (right) variance preserving spectra from ICM6 mooring 2.

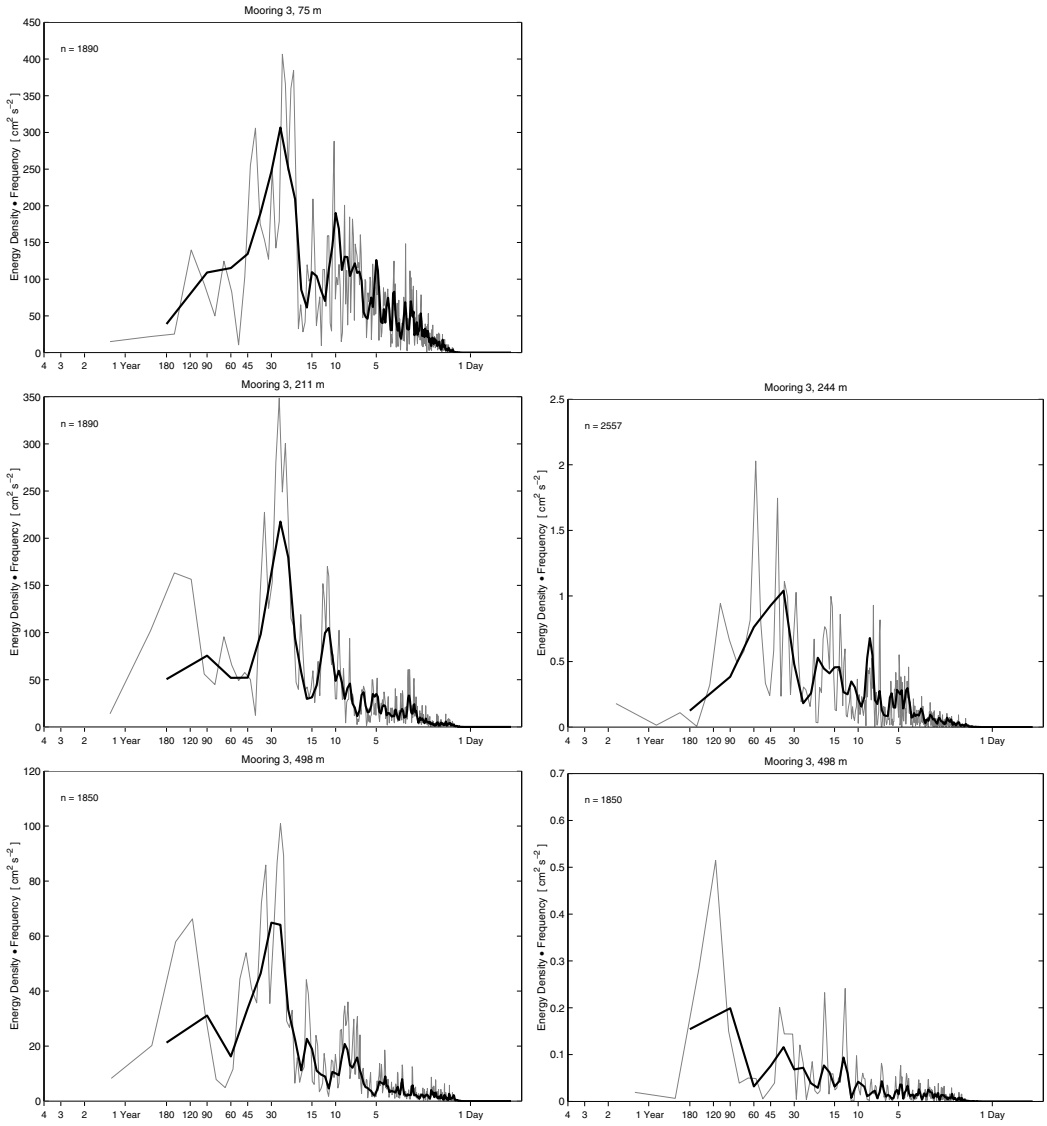

Figure A.3. Kinetic energy (left) and temperature (right) variance preserving spectra from ICM6 mooring 3.

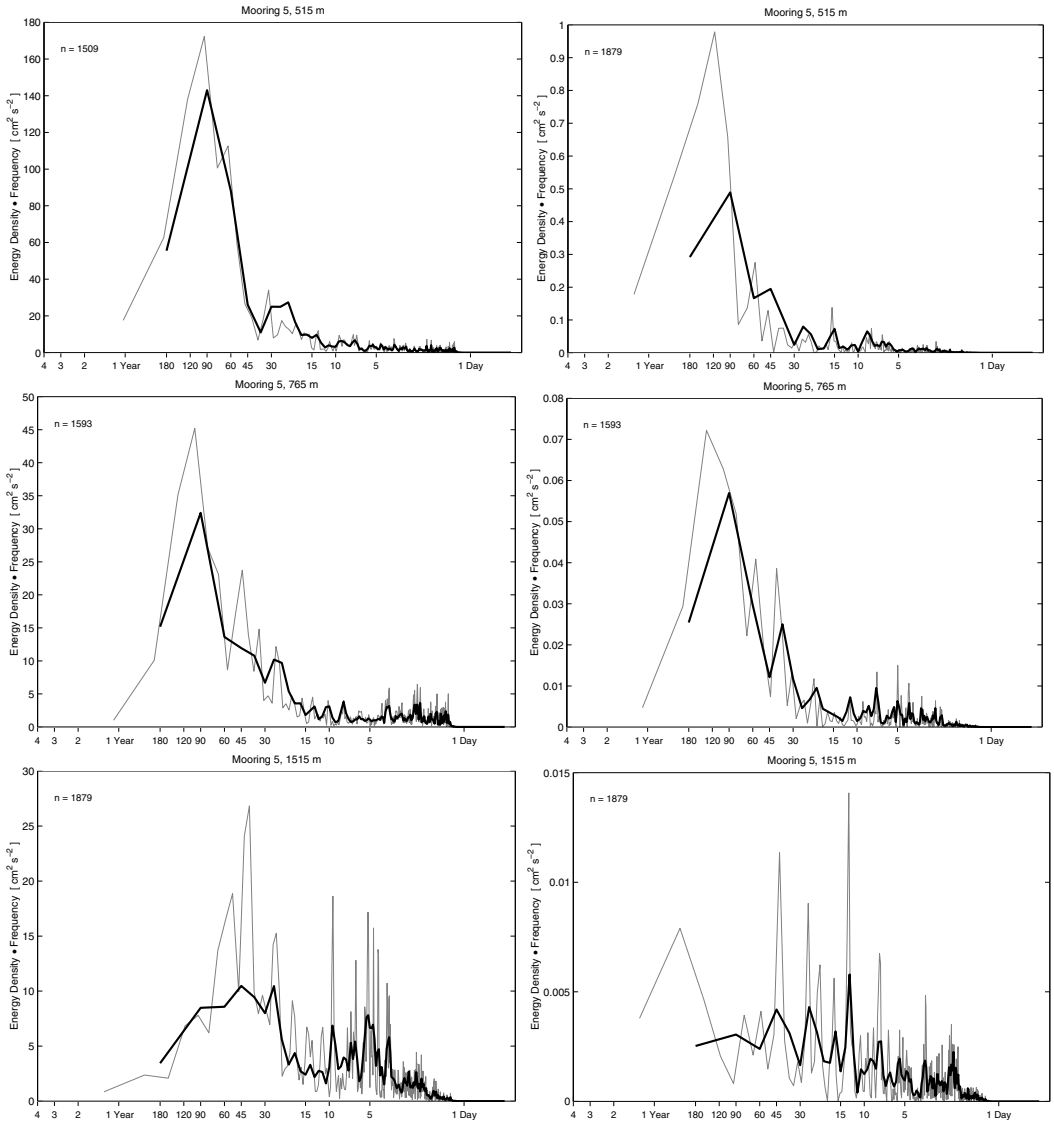

Figure A.4. Kinetic energy (left) and temperature (right) variance preserving spectra from ICM6 mooring 5.

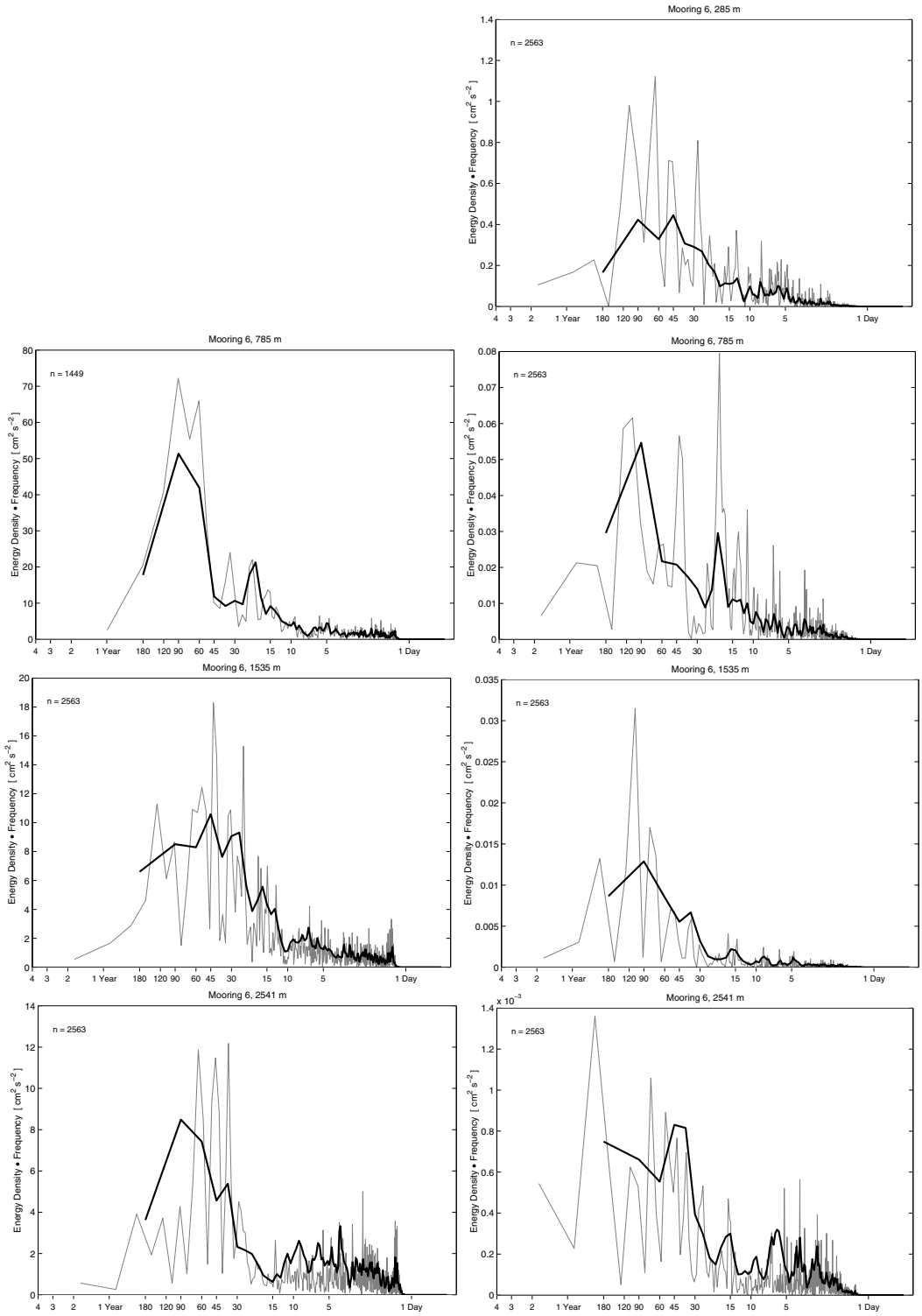

Figure A.5. Kinetic energy (left) and temperature (right) variance preserving spectra from ICM6 mooring 6.

Appendix B

ICM6 geostrophic current shears

Geostrophic current shears, perpendicular to the ICM6 array section, and relative to a level of no–motion, were diagnosed from temperature and salinity observations collected by CTD stations during surveys across the array using the thermal wind relationship. The general purpose of this type of calculation is to form full section composites of volume transport. An incorrect assumption of a level of no–motion is usually avoided by adjusting geostrophic velocity shears to direct velocity measurements, whenever possible. The thermal wind is a good approximation to the low frequency large scale circulation, however, ageostrophic processes, such as internal tides, near inertial oscillations and wind–driven Ekman currents, may cause the method to fail.

Preliminary results in Domingues *et al.* [1999b] pointed out that the thermal wind relationship at 22°S is unlikely to hold for synoptic cruise surveys, as geostrophic and direct velocity shears borne little resemblance. Ageostrophic processes, such as inertial and wind–driven Ekman currents, probably play a role in the near surface but the major problem is thought to stem from the high frequency and short wavelength disturbances of the temperature (density) field due to internal tides. Moreover, the short wavelength signal of the internal tides in the hydrographic observations can also be amplified by small distances between CTD stations. Part of the direct temperature time series on moorings 1, 2 and 3 is reproduced in **Figure B.1** to illustrate how considerably large temperature oscillations can occur in a question of hours. For instance, on mooring 1, fluctuations of 2°C to 4°C are seen in time intervals of less than 12 h (before low pass filtering). A brief examination of the current and temperature time series, before the high frequency signal was removed, suggests that the dominant internal tide components at the ICM6 site are the semi–diurnal (M2) and quarter–diurnal (M4) harmonics. Higher frequency harmonics, such as the M4, result from nonlinear interactions [Wells, 1998].

Highly variable spatial and temporal internal tides, both in amplitude and phase of currents and vertical displacements, are well known phenomena just north of the ICM6 site, along the North West Shelf [Holloway, 1983; Craig, 1988; Holloway, 1994, 1996;

Holloway *et al.*, 2001]. Their energy dissipation, through wave breaking and generation of turbulence, tends to alter the density stratification by enhancing vertical mixing, particularly near the continental shelf break and upper slope [Holloway *et al.*, 2001]. Wavelengths are typically 20–30 km [Holloway, 1996] while phases are not locked to that of the barotropic tide. In addition to tidal frequency, bottom topography and water column stratification [e.g. Holloway, 1994], the characteristics of internal tides are usually dictated by physical processes such as the configuration and variability of longshore geostrophic currents [e.g. Mooers, 1975a; Mooers, 1975b] and shelf/slope fronts [e.g. Chen *et al.*, 2003].

In an effort to reduce the ageostrophic noise verified by Domingues *et al*. [1999b], an objective mapping [Roemmich, 1983] was applied to the temperature and salinity fields prior to the thermal wind calculation. It consisted of a regularly spaced grid in depth (10 m) and longitude (0.01°), with e–folding length scales of 100 m and 2° respectively. Because the mapping imposes a certain degree of spatial smoothing, it attenuates noise but retains the large scale features relevant to geostrophy. The geostrophic current shears, constructed in this way, were then adjusted to best fit the direct velocity observations in a least squares sense. Sensitivity of the fit was tested for direct current observations, at 6 and 24 h intervals. The best matched current shears are shown in **Figure B.2** while corresponding current meter dates are listed in **Table B.1**. Note that, CTD stations from voyages FR 08/94 and FR 05/96 were not deep close to mooring 1; no simultaneous direct velocities were available for cruise surveys FR 08/94 (deployment) and FR 06/96 (recovery); early termination of the velocity observations or other instrumental malfunction did not allow shear matching for moorings 3, 5 and 6 in 1996.

Overall, except for two good matches, one on mooring 2 during FR 08/94 and another on mooring 1 during FR 06/96 leg2, the current shears have large differences, of 20 cm s^{-1} or more on occasions, as depicted by the horizontal bars (geostrophic velocity minus direct velocity) in **Figure B.2**. Even if differences appear less significant on moorings 5 and 6, the relative problem remains since the velocity amplitudes are smaller. The fit evaluation on those moorings is also complicated by the two or three point current meter observations that do not really typify a continuous vertical profile. Further attempts to reference both geostrophic and direct shears to greatest common depths (not shown) as well as averaging the hydrographic data from the different surveys altogether (not shown) before using the thermal wind relationship did little to improve the agreement. Therefore, the geostrophic current shears obtained after the objective mapping are also not reliable to further compute full sections of volume transport across the array unfortunately.

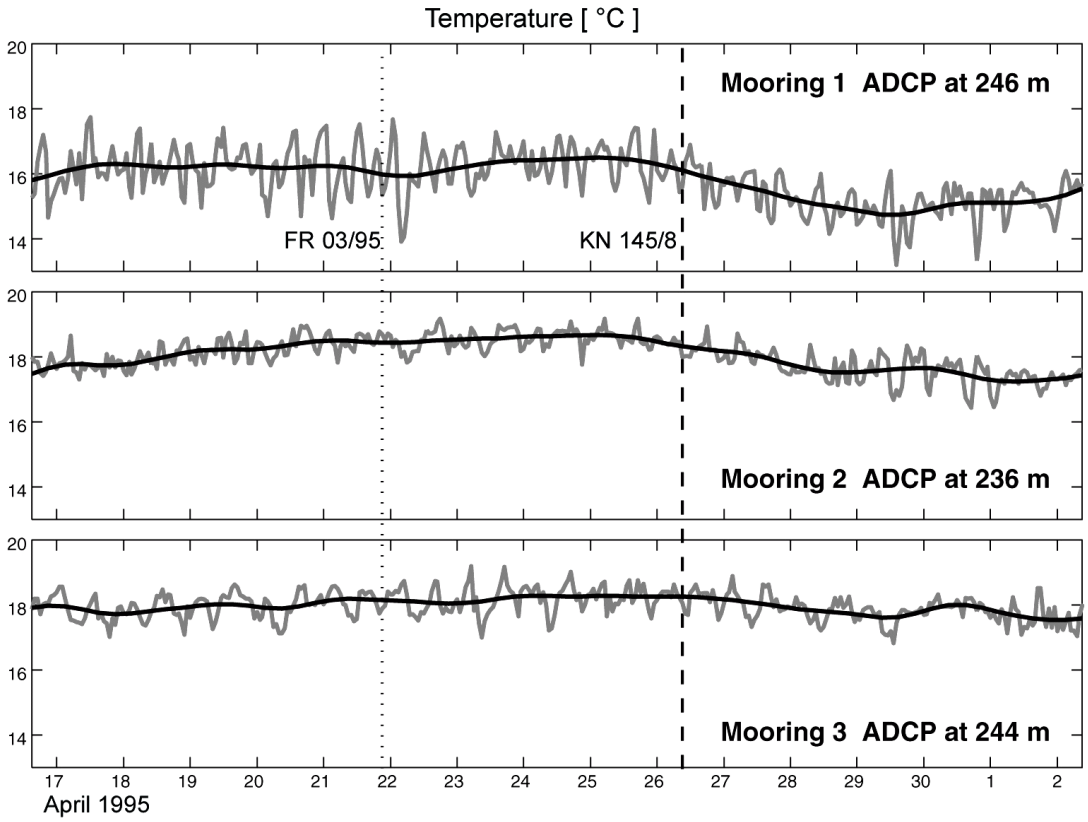

Figure B.1. Example of high frequency temperature oscillations (gray) on ICM6 moorings 1, 2 and 3 at ~250 m depth. Black line is low passed time series. Vertical lines indicate cruise dates.

Table B.1. Corresponding current meter dates for the shear matching in **Figure B.2**.

Cruises	Mooring 6	Mooring 5	Mooring 3	Mooring 2	Mooring 1
FR 08/94	30 Aug 94	01 Sep 94	30 Aug 94	01 Sep 94	30 Aug 94
FR 03/95	22 Apr 95	20 Apr 95	24 Apr 95	24 Apr 95	22 Apr 95
KN 145/8	25 Apr 95	28 Apr 95	27 Apr 95	28 Apr 95	24 Apr 95
FR 05/96	----------	----------	----------	30 May 96	27 May 96
FR 06/96 leg1	----------	----------	----------	30 May 96	30 May 96
FR 06/96 leg 2	----------	----------	----------	30 May 96	30 May 96

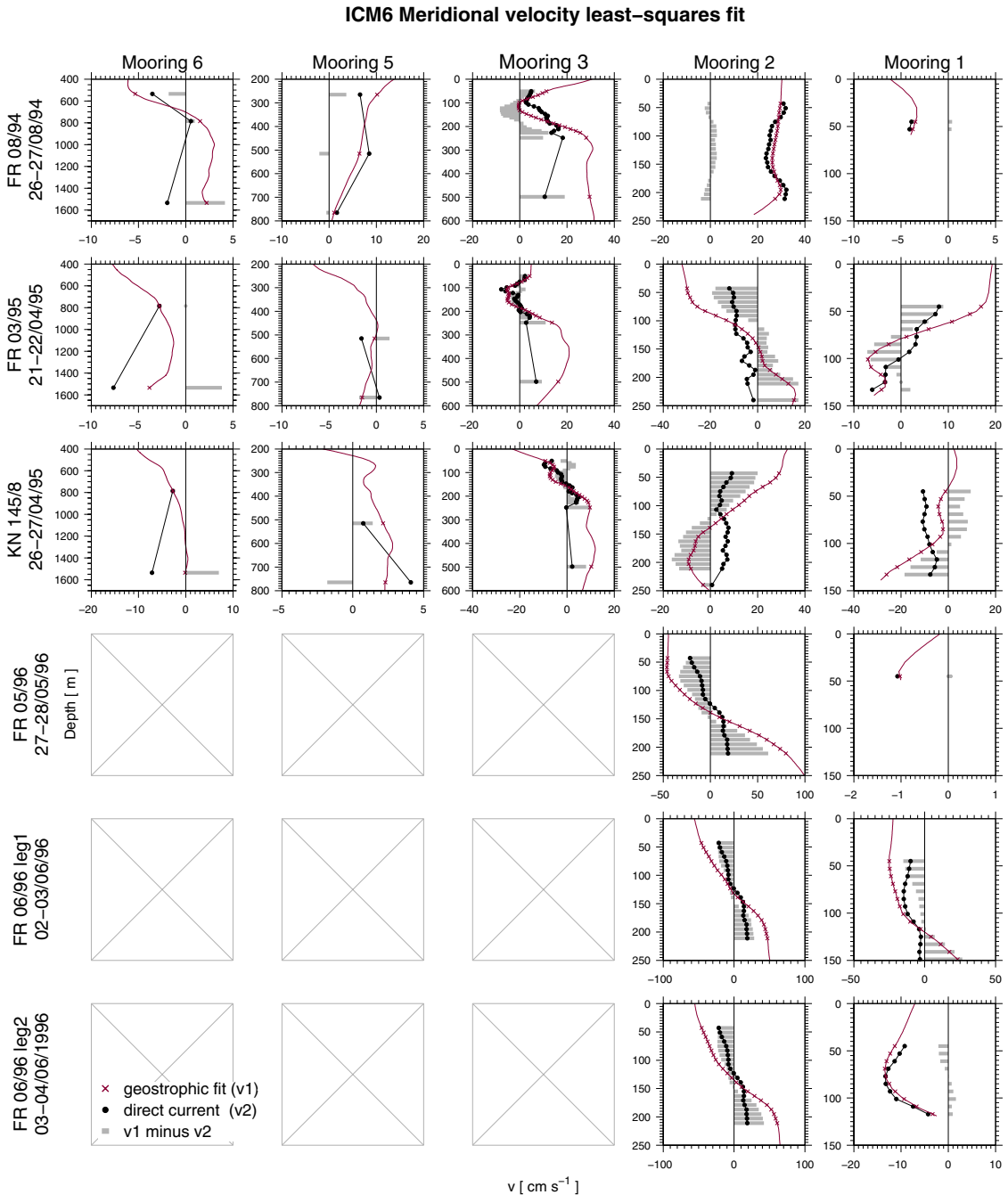

Figure B.2. Best match between geostrophic velocity shears (red crosses) and direct velocity (black dots). Horizontal gray bars indicate their differences (geostrophy minus direct). Current meter dates are listed on **Table B.1**.

Appendix C

Parallel Ocean Program model description

C.1 PARALLEL OCEAN PROGRAM

A general description of the ⅙° Parallel Ocean Program (POP) model is followed by more precise details on the POP11B simulation and on its Eulerian outputs used in this study. The technical material presented below was compiled from POP–related articles [Smith *et al.*, 1992; Dukowicz *et al.*, 1993; Dukowicz and Smith, 1994; McClean *et al.*, 1997; Maltrud *et al.*, 1998; Griffies *et al.*, 2000], POP's user guide [POP, 2002] and POP's reference manual [Smith and Gent, 2002].

C.1.1 Formulation and developments

POP initially evolved from a restructure of the multilevel Semtner–Chervin model [Semtner, 1986; Semtner and Chervin, 1988, 1992], a variant of the Bryan–Cox–Semtner code [Bryan, 1969; Semtner, 1974; Cox, 1984], matched to the array of massively parallel computers (Connection–Machine) at the Los Alamos National Laboratory [Smith *et al.*, 1992; Dukowicz *et al.*, 1993; Dukowicz and Smith, 1994]. The code was developed in Fortran 90 so as to numerically resolve the ocean system in terms of the primitive equations of momentum, continuity, tracer transport, hydrostatic principles and state, which express the primary balances of geophysical fluids. The spatial discretisation of the model subdivides the ocean into a number of horizontal and vertical computational boxes (or grid cells) wherein physical variables are arranged in a staggered B–grid [Arakawa and Lamb, 1977]. In the B–grid, tracers are placed at the midpoints of the cells, horizontal velocity at the corners and centralised in the vertical, while vertical velocities are centralised at the bottom and top surfaces of the cells [**Figure C.1**].

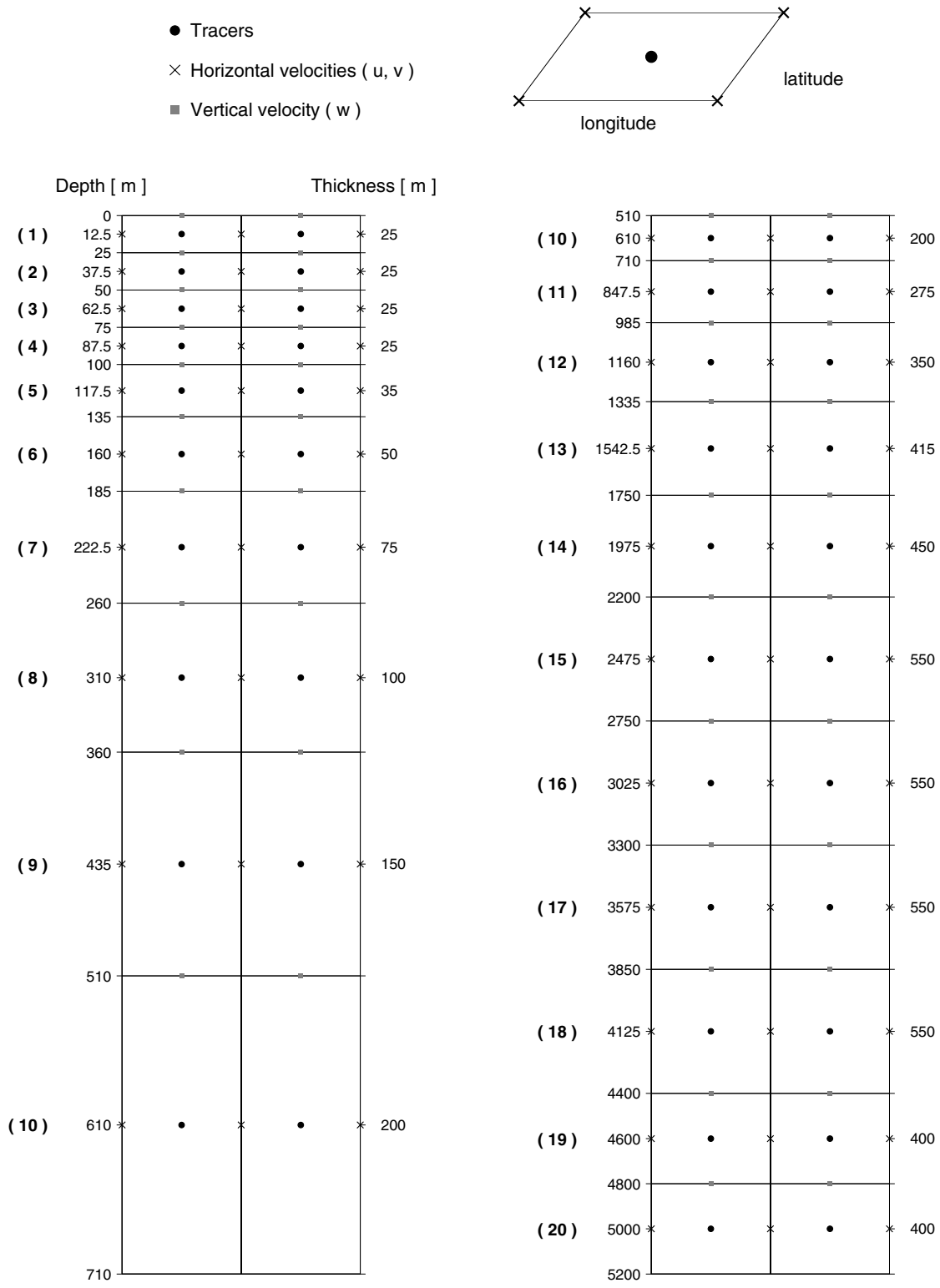

Figure C.1. POP11B horizontal and vertical B–grid cell discretisation.

The equations of motion are separated into barotropic and baroclinic modes. The barotropic mode accounts for the vertically integrated flow, which set of two dimensional elliptic equations are solved implicitly, at each model time step by numerical iteration. The baroclinic mode accounts for the departures of the primary variables (temperature, salinity and horizontal velocity) from the vertically averaged flow. Its suite of three dimensional equations is solved explicitly with a finite difference scheme, leapfrog with time–averaging [Dukowicz and Smith, 1994]. The bottom and lateral boundary conditions are no–flux (zero tracer gradient normal to boundaries), and no–slip for velocities (no flow into or along solid boundaries). Even though the no–slip condition seems the more "natural" form for the B–grid, as the velocity points lie on the boundaries, it can lead to a systematic numerical error associated with an artificial energy transfer from the barotropic to the baroclinic mode on the deep side of each topographic step [Haidvogel and Beckmann, 1999]. The active/passive advection schemes are the 2nd order centred differences as used by Bryan [1969], Semtner [1974] and Cox [1984] and QUICK scheme [Leonard, 1979] as implemented by Holland *et al.*, [1998]. To compute density from salinity and potential temperature the model uses an approximation to the UNESCO equation of state by fitting a separate cubic polynomial at each of the discrete z–levels. This polynomial approximation is only valid over a specific temperature and salinity range, and exceeding this range can lead to spurious values.

These are the developments incorporated into POP, that not only enhanced the computational performance in parallel computers but also improved the physical representation of the ocean:

- formulation of the barotropic mode in terms of surface pressure rather than the volume transport stream function;
- dismissal of the rigid lid approximation in favour of an implicit free surface formulation;
- implementation of the pressure–averaging technique for the baroclinic mode;
- latitudinal scaling of horizontal diffusion;
- discrete representation of the equations of motion in orthogonal horizontal coordinates using a displaced–pole grid.

C.1.2 POP11B 1993/97

The numerical diagnostics (or outputs) analysed in this study are from simulation POP11B. Its 5–year duration, from January 1993 to December 1997, conveniently spanned the period of the ICM6 observations (1994/96).

C.1.2.1 Geographical domain, grid structure and bottom topography

The model geographical domain covers a quasi global area, from 77°N to 77°S [**Figure C.2**], with 1280 grid points in longitude, 896 grid points in latitude, and 20 grid points in depth. The horizontal grid spacing is invariable in longitude (0.28°) but it decreases with the cosine of the latitude, cos(latitude) x 0.28°, at the same rate the diameter of typical eddies decreases, from 31.25 km (0.28°) at the equator to 6.5 km (0.06°) at the highest latitudes. This latitudinal scaling, the so called eddy–permitting resolution, is sufficient to resolve the first baroclinic Rossby radius at latitudes lower than 40°N/S [Maltrud *et al.*, 1998]. The vertical grid has 20 discrete z–levels (or geopotential surfaces), from surface to 5200 m [**Figure C.1**]. Its non–uniform thickness variation is identical to the Semtner–Chervin model [Semtner and Chervin, 1988, 1992], with 10 levels in the upper 710 m, to better represent the upper thermocline processes, and an adequate resolution near the bottom to resolve bottom pressure torques. POP11B adopts the digital terrain 1/12° (5') ETOPO5 bathymetry database from the *National Geophysical Data Center* [NGDC, 1988] interpolated to its B–grid. Therefore the model bottom topography retains a step–like structure consistent with the z–levels in **Figure C.1**.

C.1.2.2 Initialisation

POP11B (January 1993 to December 1997) is an extension of a previous run, POP11 (January 1985 to December 1995). Initial thermohaline fields interpolated to the 1/6° POP11 were obtained from the end state of the 3–year 1/4° simulation [Semtner, 1998], in turn initialised by a 32.5–year integration of an 1/2° simulation [Semtner and Chervin, 1992], and then spun up from rest for 5 years [**Figure C.3**]. Although this model initialisation draws near dynamic equilibrium – defined as a statistically steady state wherein the running mean of the total energy of the system has approached some constant or slowly varying level – it may introduce problems presented in prior simulations, such as the warming of the thermocline waters by a few degrees [Maltrud *et al.*, 1998]. According to Haidvogel and Beckmann [1999] a 20–25 year integration period from rest in an eddy–permitting resolution would be required to achieve dynamic equilibrium.

C.1.2.3 Surface forcing

The model is forced with wind stress, heat and freshwater fluxes in the upper 25 m (surface cell). The thickness of the surface cell is constant but changes in the free sea surface height are taken into account in the forcing terms. As a result, freshwater fluxes are deemed virtual salinity fluxes and conservation of tracers is not exact (though the residual tracer flux is globally very small). Because presently available heat and salt

forcing products still contain inaccuracies, the forcing terms in the model equations are restored to climatological values (relaxation), over a fixed and/or variable timescale, to produce more realistic conditions. The relaxation depends on the difference between the climatological value and the current model value. Although the actual forcing terms are evaluated at every model time step, the value that is being restored to stays constant over a certain timescale. The forcing products are:

- Wind stress – daily averaged 10–m wind stress from the six–hourly European Centre for Medium–Range Weather Forecasts (ECMWF) 1985/95 analyses at a 2.5° horizontal resolution interpolated to the model grid.

- Surface heat flux – seasonally varying heat fluxes from the six–hourly 1986/88 ECMWF surface atmospheric field analyses at a 1.125° horizontal resolution interpolated to the model grid. The formulation of the surface heat flux is discussed in Barnier *et al.* [1995]. Effective surface heat fluxes are a sum of the ECMWF fluxes plus a relaxation flux, where the relaxation timescale varied spatially from 20 to 65 days. At high latitudes, in assumed ice cover areas, the sea surface temperature was restored to –2°C with a 1–month relaxation timescale.

- Surface freshwater flux – daily averaged effective freshwater fluxes, precipitation minus evaporation [P–E], are parameterised by restoring the surface salinity to the monthly Levitus climatology [Levitus, 1982] with a 1–month relaxation timescale.

C.1.2.4 Deep restoring

Deep restoring takes place only poleward of 70°N/S (buffer zones), where temperature and salinity are relaxed to an annual mean climatology [Levitus, 1982] from surface to 2000 m with a 3–year relaxation timescale.

C.1.2.5 Subgridscale parameterisation

Effects of small scale processes (i.e., molecular diffusion and viscosity, turbulence and convection) on large scale systems that cannot be explicitly resolved are implicitly represented via parameterisations:

- Lateral mixing – horizontal mixing of momentum and tracers is parameterised using biharmonic coefficients with latitudinal scaling to assure that the amount of friction in a given length is independent of horizontal location. The spatially varying viscosity and diffusivity mixing coefficients are $-6.0 \times 10^{19} \cos^3$ (latitude) cm^4s^{-1} and $-2.0 \times 10^{19} \cos^3$ (latitude) cm^4s^{-1} respectively.

- Vertical mixing – based upon the gradient Richardson number [Pacanowski and Philander, 1981]. The vertical diffusivity and viscosity are influenced by both stratification and vertical current shear, and thus functions of the Richardson number. The background vertical viscosity and diffusivity and the Richardson number function coefficients are 1.0 cm^2s^{-1}, 0.1 cm^2s^{-1} and 50 respectively.

- Mixed layer – turbulent kinetic energy produced by wind stress and heat/salt (buoyancy) fluxes at the surface is converted into potential energy through stirring and mixing of water properties, primarily in the vertical. To implicitly account for this, POP11B relies on the Pacanowski and Philander [1981] vertical mixing scheme. There is no explicit mixed layer scheme (e.g., slab model).

- Convection – parameterised using a convective adjustment to remove statically unstable water columns by instantaneously mixing tracers until all unstable stratification occurrences vanish.

- Bottom friction – approximated by a conventional quadratic stress law (drag coefficient = $1.225\ 10^{-3}$) to represent momentum transfer at the seafloor. The bottom drag acts directly only on the cell immediately adjacent to the bottom. Cells higher in the water column "feel" the bottom friction through the resulting vertical shear and vertical eddy viscosity.

C.1.2.6 Eulerian outputs

POP11B outputs encompass an extensive inventory of 32–bit single precision diagnostics, from forcings and primary variables to second moments, between January 1993 and December 1997, stored in different temporal resolutions and file formats. For this study, we have requested monthly mean files in netCDF format via POP's website [*http://climate.lanl.gov/Models/POP/index.htm/*] for a specific region of the southeast Indian Ocean, between 10°N and 40°S and 80°E and 150°E [**Figure C.2**]. These files were assigned to a file–transfer–protocol system by Robert Malone and Matthew Maltrud. The monthly mean outputs are time averages constructed by accumulating in memory at each time step the running sums of selected diagnostics or correlation of diagnostics. The diagnostics analysed in this study may include net surface heat flux (SHF), wind stress (τ), sea surface height (SSH, SSH^2), velocity (u,v,w), potential temperature (θ), salinity (S), potential density referenced to surface (σ_θ), and zonal and meridional fluxes of potential temperature ($u\theta$, $v\theta$). The formula to calculate SSH variance is:

$$\text{variance} = [\, N(x_1^2 + x_2^2 + x_3^2 + \ldots + x_N^2) - (x_1 + x_2 + x_3 + \ldots + x_N)^2]\, N^{-2} \quad \text{[Equation D.1]}$$

where: x is SSH, x^2 is SSH^2 and N is month number.

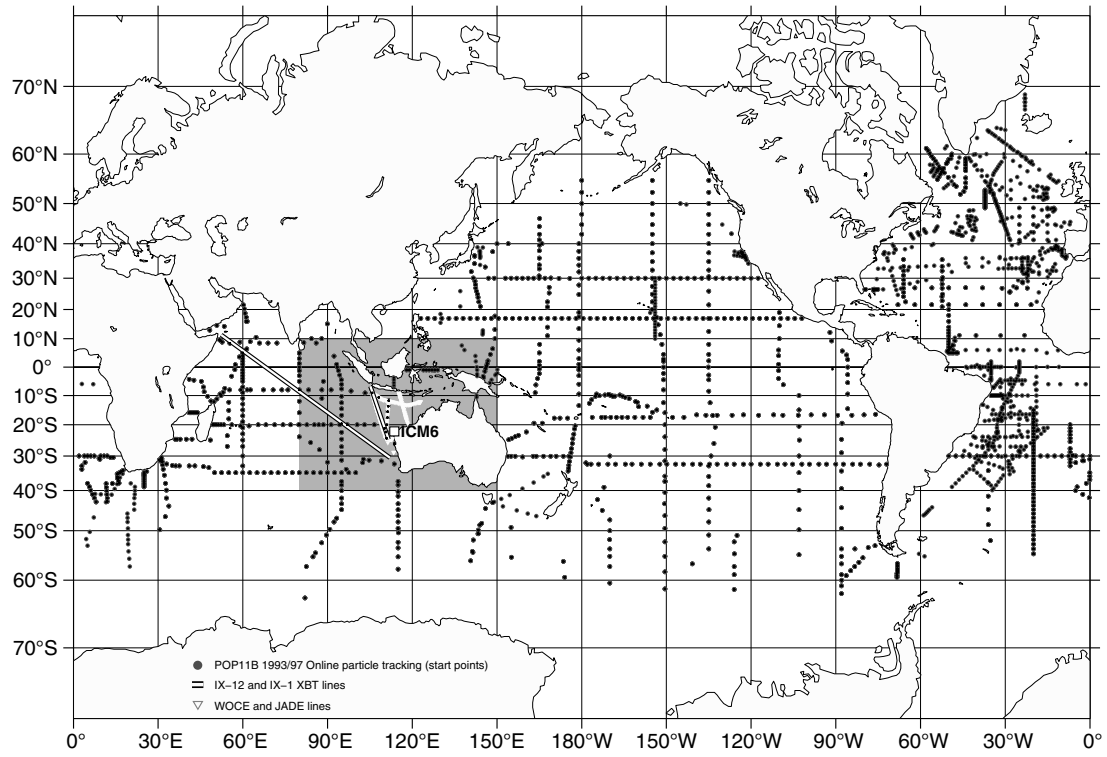

Figure C.2. POP11B global grid in Mercator projection. The study area in the southeast Indian Ocean is highlighted in gray [Eulerian diagnostics used in **Chapters 5** and **6**]. Also indicated are the locations of the start points for the numerical particle tracking [online Lagrangian diagnostics in **Chapter 4**], the ICM6 current meter array, the JADE and WOCE hydrographic lines, and the IX–1 and IX–22 XBT lines [**Chapter 3**].

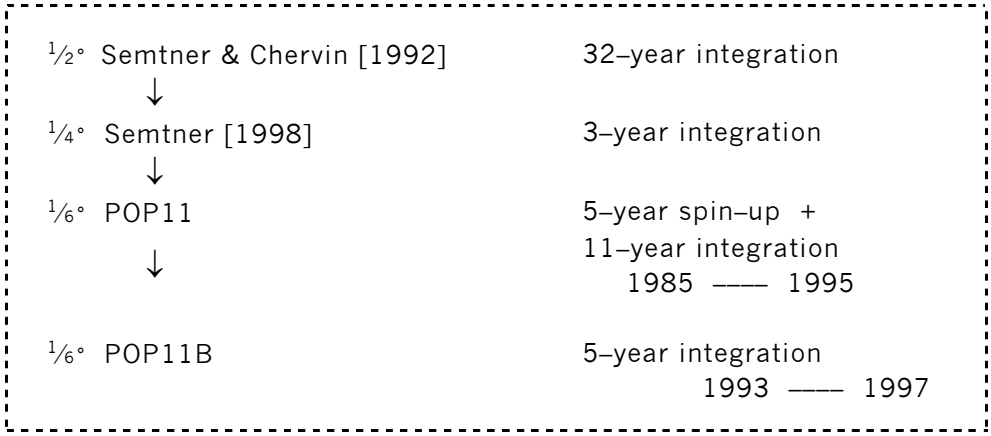

Figure C.3. POP11B initialisation schematic diagram.

Appendix D

Regional heat balance

In this appendix we present the storage+diffusion and volume (mass) flux components of the heat balance off Western Australia [**Chapter 6**], integrated from top to bottom, over 1° x 1° boxes for the region between 20°–38°S and 100°–125°E.

We also present the depth–integrated ocean heat transport (mean and eddy) for the coastal and offshore boxes.

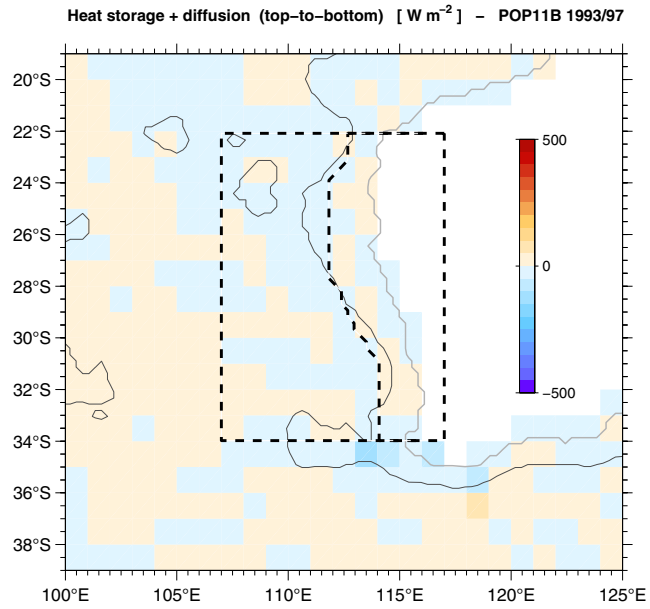

Figure D.1. Storage+diffusion over 1° x °1 boxes off Western Australia. The gray bold line is the model coastline whereas the thin gray line is the model 3000 m isobath. Dashed lines are the coastal and offshore boxes used in a previous calculation of the heat balance in those areas [see **Chapter 6** for details]. Positive values indicate heat storage in the ocean. Note that the estimates for the 5–year period (1993/97) are quite small and so the model is in a dynamical steady state.

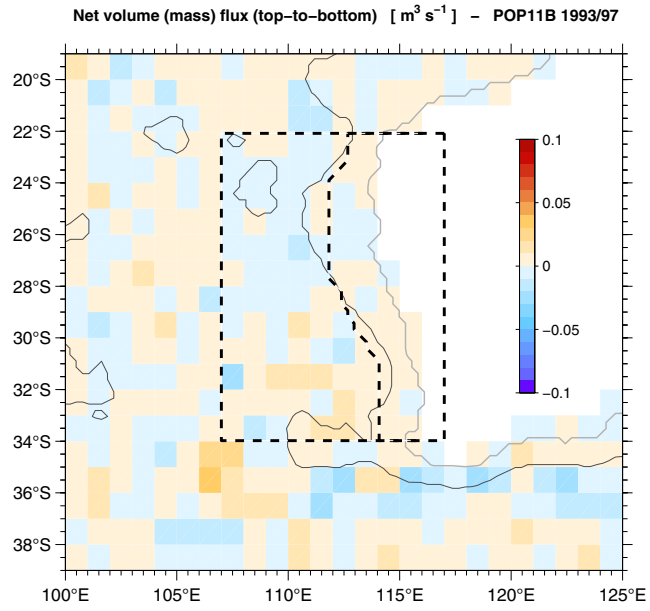

Figure D.2. Same as above but for net volume (mass) flux. Positive values indicate mass flux into the boxes. Note, however, that the estimates in each of the 1° x 1° boxes are ~0 Sv (≡10^{-6} m^3 s^{-1}), hence there is virtually no net mass flux (thus mass balance is closed).

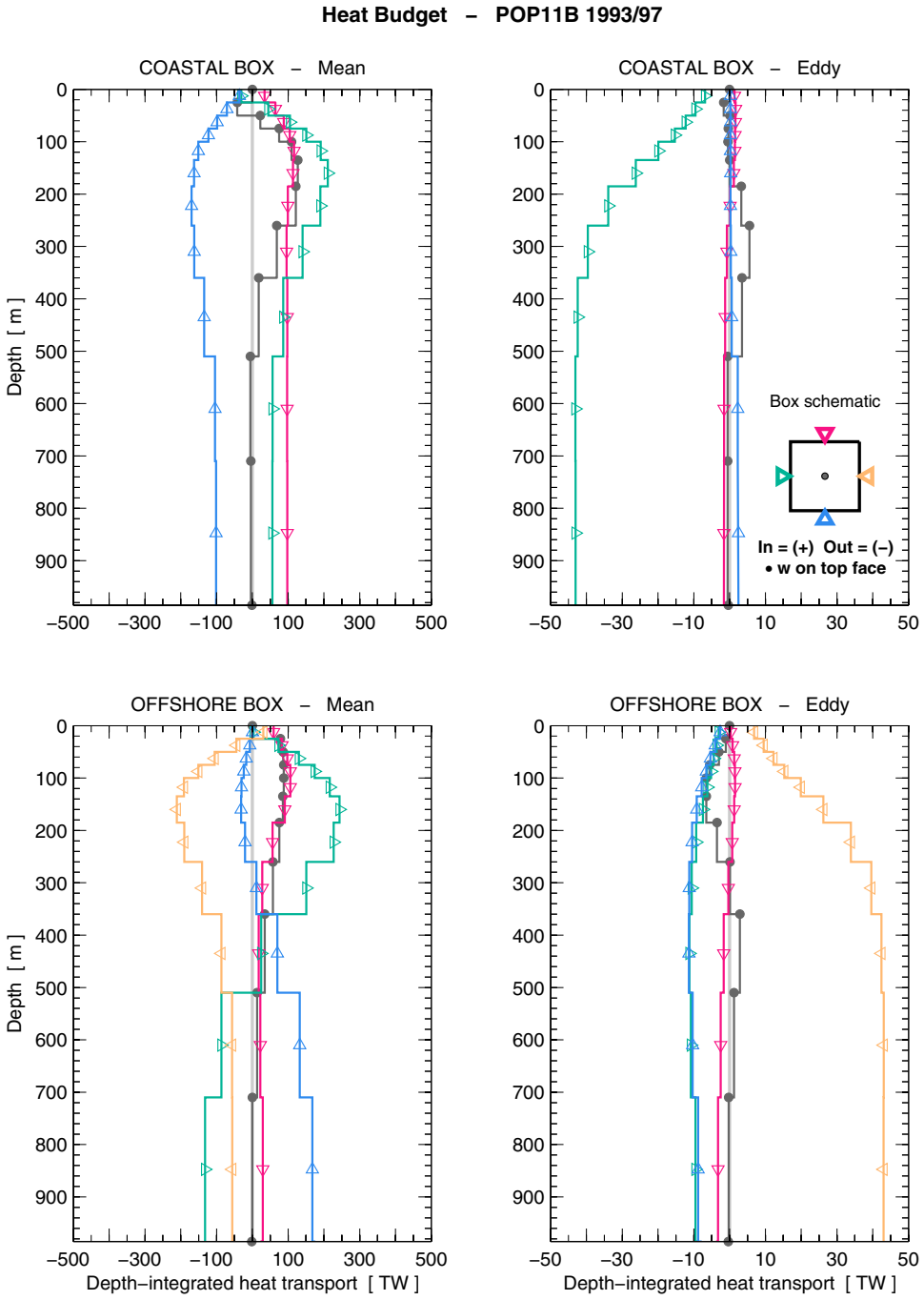

Figure D.3. Depth–integrated ocean heat transport (mean and eddy) in each of the faces of the coastal and offshore boxes, as indicated by colour and symbols. The heat transport values at ~1000 m are equivalent to the full depth integration (0–5200 m)